

Phase measurements without interferometry: 2D transverse phase detection by numerical beam intensity analysis

By P. CHESSA,** M. GALIMBERTI,* A. BARBINI,*
C.N. DANSON,† A. GIULIETTI,* D. GIULIETTI,††
AND L. GIZZI*

*IFAM-CNR, Via del Giardino, 7, 56127 Pisa, Italy

**LOA-ENSTA, Ecole polytechnique, 91128 Palaiseau cedex, France

†CLF, Rutherford Appleton Laboratory, Chilton, Didcot, Oxon OX11 0QX, UK

††Dipartimento di Fisica, Università degli Studi, Piazza Torricelli, 2, 56100 Pisa, Italy

(Received 4 August 1998; Accepted 14 January 1999)

A whole family of laser-plasma interaction experiments is based on the phase analysis of the laser pulse after the propagation in a plasma. Typically, this phase is obtained by means of interferometry. As pulsed interferometry is a much more difficult task than taking simple images of the beam, we developed a numerical code for extracting phase information from images. The technique, based on the algorithm of Gerchberg–Saxton, showed to be very effective in retrieving 2D phase distributions of simulated as well as real beams. The convergence of the algorithm is fast (some minutes on a personal computer). The electronic noise in real images is intrinsically discarded by the algorithm.

1. Introduction

A typical concern of laser-plasma physicists is the observation of the phase of an interacting or a probe laser pulse after the propagation in a plasma. The pulse spectral shift gives, for instance, information about plasma density evolution in time (Le Blanc *et al.* 1993; Giulietti *et al.* 1994). Fine techniques have been developed in the time domain in order to measure phase differences between probe pulses with high phase resolution (Marquès *et al.* 1997). The retrieval of the spatial phase distribution is usually performed by means of interferometry (Gizzi *et al.* 1994; Borghesi *et al.* 1997). This typically needs two identical laser pulses with initial good optical quality, synchronization of pulses, and a wide angle imaging system for the interference region. This technique demands, by far, a greater effort than taking simple photographs of the beam intensity distribution.

Optical phase retrieval from intensity distributions has been already tested on scattered light in diffraction tomography experiments (Maleki & Devaney 1993). We present a preliminary study for the application of the numerical phase retrieving in the domain of laser interaction physics.

2. Basic algorithm

Some phase retrieving algorithms have been proposed during the last years. The simplest one is the so-called Gerchberg–Saxton (Gerchberg & Saxton 1972, Fienup 1982) algorithm. The flux diagram in figure 1 shows the principle of this algorithm.

Two intensity distributions $I^{(1)}$ and $I^{(2)}$ are known experimentally. The direct and inverse propagation operators P and P^{-1} transform the input field E^1 into the output $E^{(2)}$ and *vice-*

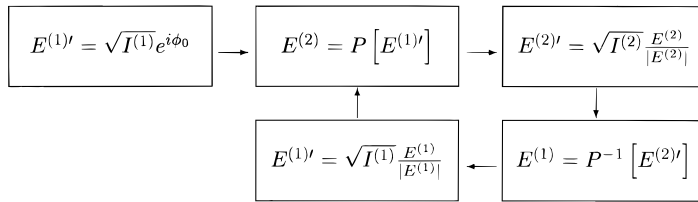


FIGURE 1. Flux diagram of the Gerchberg–Saxton algorithm. $I^{(1)}$ and $I^{(2)}$ are the measured intensity distributions, $E^{(1)}$ and $E^{(2)}$ are the corresponding fields, P and P^{-1} are the direct and inverse propagation operators and ϕ_0 is the guessed phase at the input plane.

versa. An initial phase distribution ϕ_0 is guessed to build the candidate input complex field $E^{1'}$ up. Then the corresponding output field $E^{(2)}$ is worked out, and its amplitude distribution replaced by the experimental one $\sqrt{I^{(2)}}$. The loop is closed by propagating the new output field $E^{(2)'}$ backwards and setting the amplitude of the input field $E^{1'}$ equal to the experimental one.

As a general rule, the phase retrieving algorithms are based upon the minimization of the functional error (Ivanov *et al.* 1992)

$$\hat{J} = \sum_i \iint_{-\infty}^{+\infty} (E^{(i)} - \sqrt{I^{(i)}})^2 dx dy. \quad (1)$$

Although the Gerchberg–Saxton algorithm does not require to compute any functional gradient, it can be shown that, in the vicinity of the solution, it converges with the same speed as the traditional steepest gradient algorithm (Ivanov *et al.* 1992). Yet, compared to the explicit calculation of the functional gradient of the error \hat{J} , the Gerchberg–Saxton algorithm has the advantage of simplicity and of a minimum number of computations per step. In a similar but simplest context (1D), the same algorithm has been successfully applied for the frequency resolved optical gating (FROG) time phase control of short laser pulses (Trebino & Kane 1993). We have then chosen to implement the Gerchberg–Saxton algorithm and to test it with typical 2D phase retrieving problems.

In order to compare test results with a known phase distribution, we choose to retrieve the phase imprinted on a focused beam by a random phase plate (RPP) (Kato *et al.* 1984; Pepler *et al.* 1993). This is an optically flat plate divided into square cells, a random selection of which is coated with a thin dielectric layer. By controlling the thickness of the layer, one can introduce a wanted optical path difference between the coated and the uncoated cells. Tests will be presented here, where the pattern and the phase step of the RPP are retrieved from the images of simulated as well as real He-Ne laser beams.

3. Phase retrieving from two images

For the first test we take two images of a simulated Gaussian beam passing through a positive lens and a RPP located in the same plane. The beam wavelength and intensity FWHM diameter on the lens are $\lambda = 1.064 \mu\text{m}$ and $d_{\text{beam}} = 2.35 \text{ cm}$ respectively, and its input phase is set flat. The focal length is $f = 24 \text{ cm}$, and the RPP phase step and cell size are $\Delta\phi = \pi$ and $s_{\text{cell}} = 1 \text{ cm}$ respectively. The two pictures shown in figure 2 are taken at the RPP plane and at the focal plane of the lens respectively. The resolutions of the two images are $dx_1 = 880 \mu\text{m}$ and $dx_2 = 0.57 \mu\text{m}$ respectively.

In this case, the algorithm falls into numerical stagnation (Fienup & Wackerman 1986) and the RPP shape can not be retrieved even after thousands of iterations (figure 3). This is a typical behavior of algorithms solving the phase retrieval problem from two images (Ivanov *et al.*

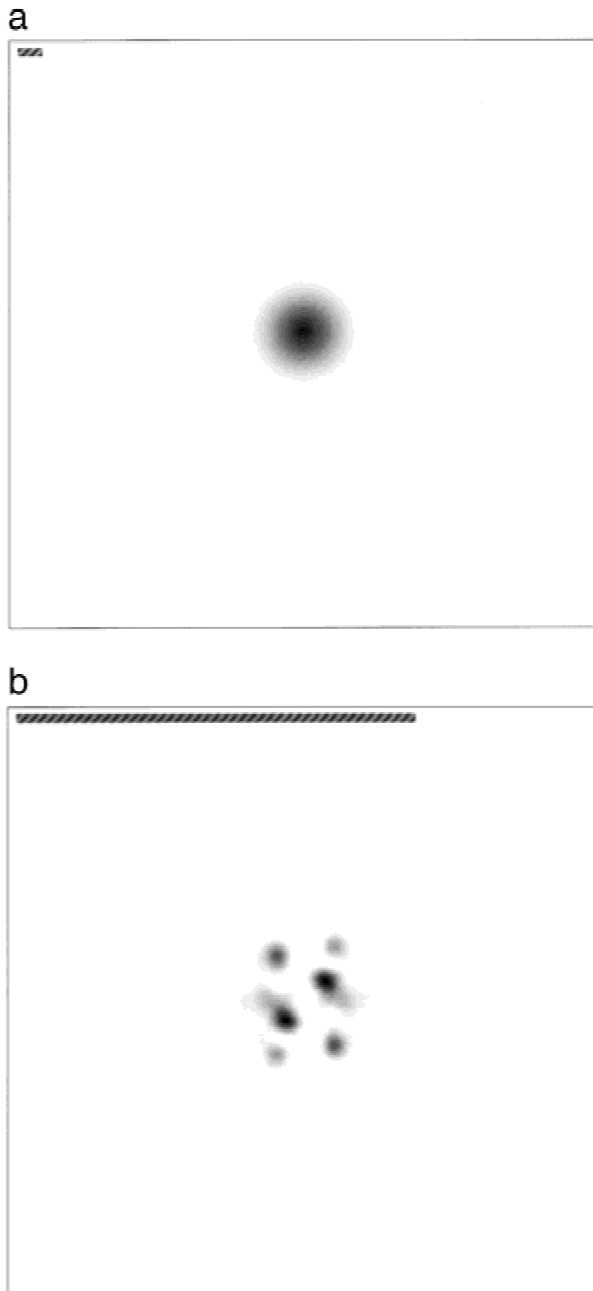


FIGURE 2. Simulated test images of a laser beam ($\lambda = 1.064 \mu\text{m}$) focused by a positive lens ($f = 24 \text{ cm}$) through a random phase plate (RPP). (a)—beam intensity just after the plane where the focusing lens and the RPP lie; (b)—beam intensity at the focal plane of the lens. Reference bar length: $l_{\text{bar}} = 1 \text{ cm}$, for (a); $l_{\text{bar}} = 100 \mu\text{m}$, for (b).

1992). As a matter of fact, this problem has in general an infinite number of solutions. An example of multiple solution follows.

Let's consider an incoming beam with a Gaussian intensity distribution and a flat phase focused by an astigmatic lens of main focal lengths f_1 and f_2 . In this case, we can write the complex field after the lens as

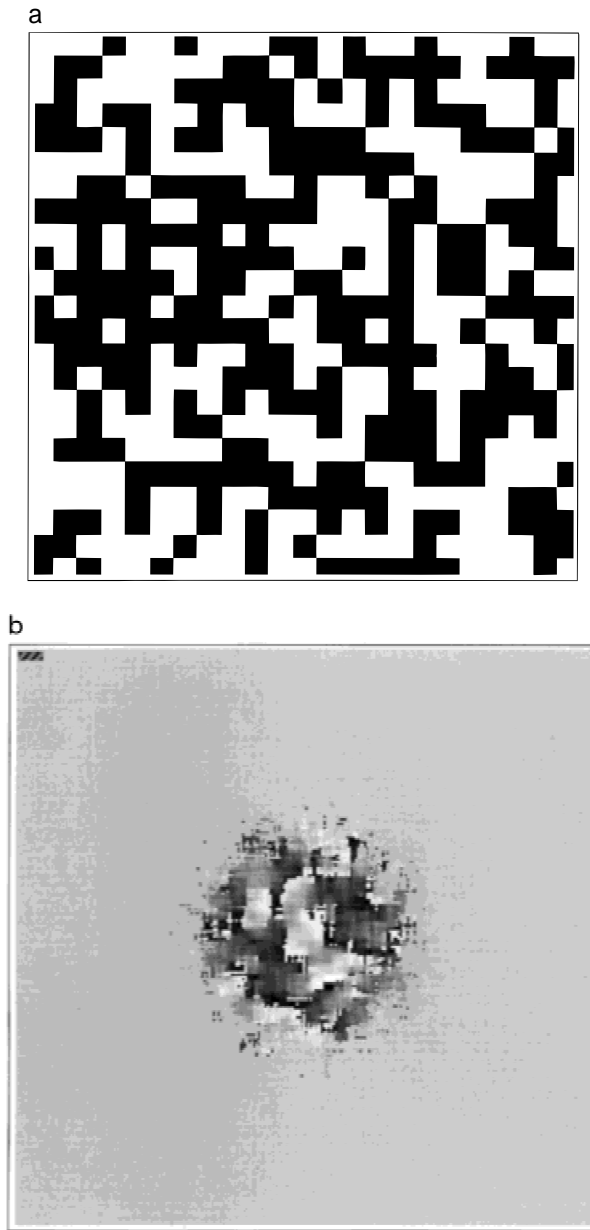


FIGURE 3. (a)—RPP pattern; (b)—retrieved phase at the plane of the RPP after 5000 iterations. (a)—cell size $s = 1$ cm; phase step $\Delta\phi = \pi$. (b)—gray-map $[-\pi, \pi] \rightarrow [white, black]$; reference bar length $l_{\text{bar}} = 1$ cm. Phase is retrieved close to the beam axis, where the amplitude of the field exceeds the numerical noise of the calculation. The retrieved phase in (b) does not contain the parabolic phase of the lens.

$$E = E_0 \exp\left(-\frac{x^2 + y^2}{w^2}\right) \exp\left[-i \frac{k}{2} \left(\frac{x^2}{f_1} + \frac{y^2}{f_2}\right)\right], \quad (2)$$

where w^2 is the variance of the 2D amplitude distribution at the lens and the coordinate system has been chosen in order to match the lens axes.

It is known that the propagation of a beam can be worked out by the paraxial development of the Kirchhoff integral, giving

$$E(x, y, z) = \frac{k \exp\left(ik \frac{x^2 + y^2}{2z}\right)}{2\pi iz} \iint_{-\infty}^{+\infty} E(x', y', 0) \exp\left(ik \frac{x'^2 + y'^2}{2z} - ik \frac{xx' + yy'}{z}\right) dx' dy'. \quad (3)$$

So, when the beam field formula is put into the integral, variables get separated and we can write

$$E(x, y, z) = E_0 \frac{k}{2\pi iz} \exp\left(i \frac{k}{2} \frac{x^2}{z}\right) \int_{-\infty}^{+\infty} \exp\left(-\frac{x'^2}{w^2} - i \frac{k}{2} \frac{x'^2}{f_1} + i \frac{k}{2} \frac{x'^2}{z} - ik \frac{xx'}{z}\right) dx' \\ \times \exp\left(i \frac{k}{2} \frac{y^2}{z}\right) \int_{-\infty}^{+\infty} \exp\left(-\frac{y'^2}{w^2} - i \frac{k}{2} \frac{y'^2}{f_2} + i \frac{k}{2} \frac{y'^2}{z} - ik \frac{yy'}{z}\right) dy'. \quad (4)$$

When $f_1 = f_2 = f$, this gives the usual Gaussian beam propagation. Taking the astigmatism into account, a beam is defined whose amplitude distributions along the x and y directions respectively are Gaussian everywhere, with a line focus in the y direction close to the position $z = f_1$ (if $kw^2 \ll 2f_1$) and an other in x direction at about $z = f_2$ (if $kw^2 \ll 2f_2$). In the region between the linear foci, the standard deviations $w_x(z)/\sqrt{2}$ and $w_y(z)/\sqrt{2}$ of the two transverse amplitude distributions grow in opposite senses. So, at position

$$z_f = 2 \frac{f_1 f_2}{f_1 + f_2}, \quad (5)$$

between the two line foci, it is found that $w_x = w_y$. Like at the lens plane, the overall field amplitude distribution for $z = z_f$ comes out to be a Gaussian function of the radius $r = \sqrt{x^2 + y^2}$.

Let's now consider the problem of retrieving the phase of a Gaussian beam by the images of two planes at a distance z . Let the standard deviation of the amplitude distributions be at these positions $w_1/\sqrt{2}$ and $w_2/\sqrt{2}$ respectively. From the above discussion, it comes out that the two images are then consistent with an astigmatic beam coming from a lens of main focal lengths f_1 and f_2 , as given by equation (6).

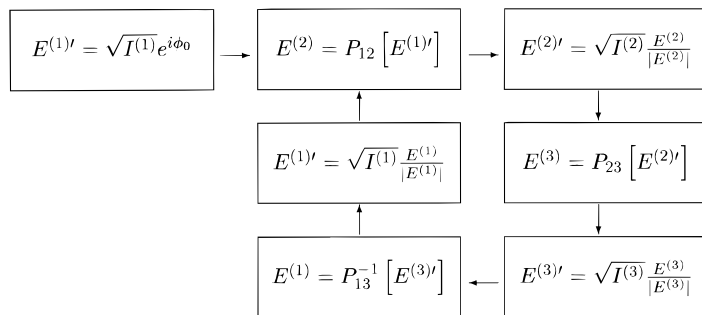


FIGURE 4. Flux diagram for three test images. Index (1), (2), and (3) mark the input, intermediate and output plane respectively. P_{12} , P_{23} , and P_{13}^{-1} are the operators of propagation from the input to the intermediate plane, from the intermediate to the output plane, and from the output backwards to the input plane respectively. The initial phase ϕ_0 is guessed at the input plane.

$$\frac{1}{f_1} = \frac{1}{z} + \frac{2}{kw_1} \sqrt{\left(\frac{kw_2^2}{2z}\right)^2 - \frac{1}{w_1^2}}$$

$$\frac{1}{f_2} = \frac{1}{z} - \frac{2}{kw_1} \sqrt{\left(\frac{kw_2^2}{2z}\right)^2 - \frac{1}{w_1^2}}. \quad (6)$$

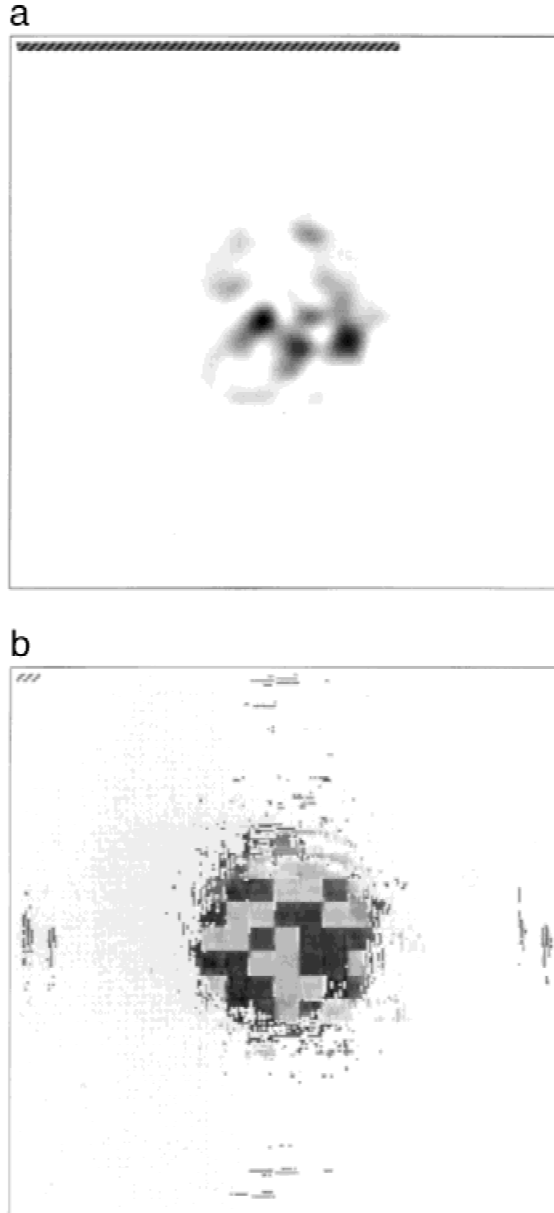


FIGURE 5. (a)—beam intensity $200 \mu\text{m}$ before the focal plane of the lens, for the same beam as in figure 2; (b)—retrieved phase at the plane of the RPP. (a)—reference bar length $l_{\text{bar}} = 100 \mu\text{m}$. (b)—reference bar length $l_{\text{bar}} = 1 \text{ cm}$, gray-map $[-\pi, \pi] \rightarrow [\text{white}, \text{black}]$. The retrieved phase in (b) does not contain the parabolic phase of the lens. A phase step $\Delta\phi_{\text{retr}} = \pi(1 \pm 1/256)$ between the squared cells is retrieved from (b).

This solution exists for any choice of w_1 and w_2 provided that they are consistent with the diffraction limit. It defines an infinite family of astigmatic beams that, regardless of the cylinder axis, match the same two images taken along the propagation of a Gaussian beam. We conclude that the problem of the retrieving phase from two images has, in general, degenerated solutions that prevent the phase-retrieving algorithm from converging. Some supplemental information must then be added to the two images.

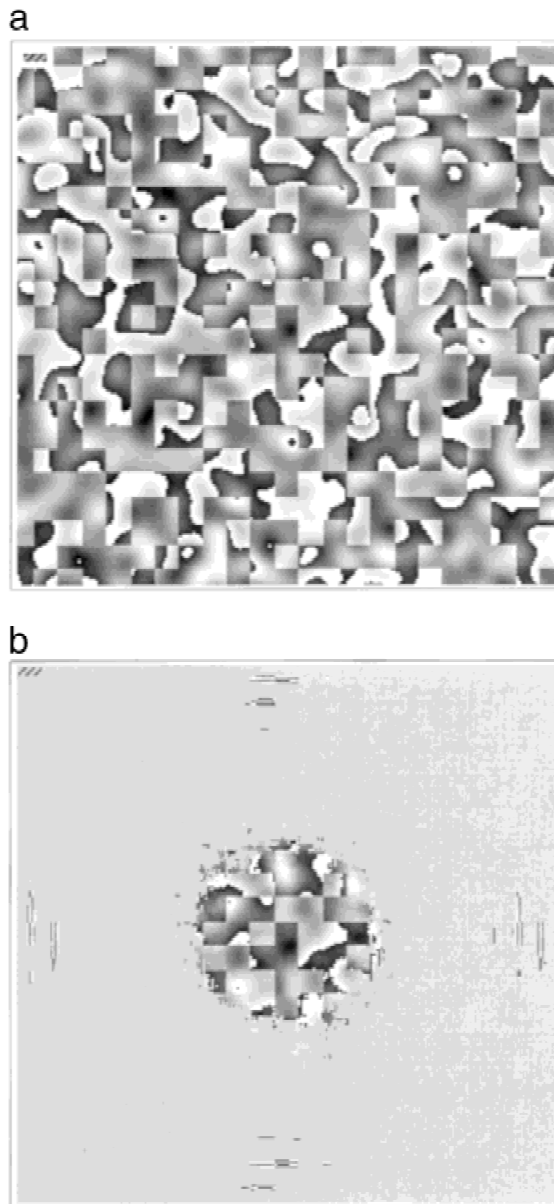


FIGURE 6. Input and retrieved phase distributions at the plane of the RPP. (a)—input phase distribution; (b)—retrieved phase distribution. Reference bar lengths: $l_{\text{bar}} = 1$ cm. Gray-map: $[-\pi, \pi] \rightarrow [\text{white}, \text{black}]$. The phase distributions do not contain the parabolic phase of the lens.

4. Phase retrieving from more than two images

The following step consists of taking more than two images. The flux diagram must then be modified like in figure 4 where a third field $E^{(3)}$ has been introduced in the loop and the propagation operators P and P^{-1} have been replaced by the partial propagation operators P_{12} ,

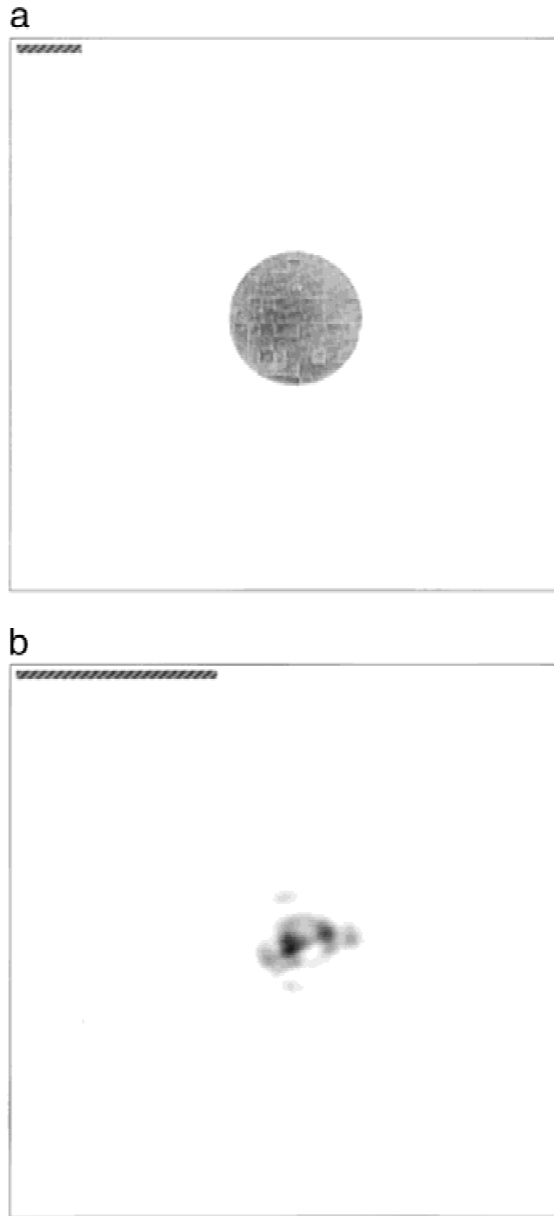


FIGURE 7. Experimental test images of a laser beam ($\lambda = 0.633 \mu\text{m}$) focused by a lens ($f = 80 \text{ cm}$) through a RPP. (a)—beam intensity distribution just after the plane of the RPP; (b)—beam intensity distribution 2.45 cm before the focal plane of the lens; (c)—beam intensity distribution at the focal plane of the lens. Reference bar length: $l_{\text{bar}} = 0.5 \text{ cm}$ (a); $l_{\text{bar}} = 500 \mu\text{m}$ for figures (b) and (c). Distance from the phase plate: $z_1 = 0$ for figure (a); $z_2 = 75.05 \text{ cm}$ for figure (b); $z_2 = 77.5 \text{ cm}$ for figure (c). (*Figure continues on facing page.*)

P_{23} and P_{13}^{-1} . In Figure 5(a), a simulated intensity distribution is shown, corresponding to an intermediate plane in the propagation of the beam of figure 2. The distance from the phase plate is in this case $z_3 = 23.98$ cm, corresponding to a plane located $200 \mu\text{m}$ before the focal plane of the lens. The spatial resolution is the same as for figure 2b, $\delta x_3 = 0.57 \mu\text{m}$. The retrieved phase at the plane of the plate is shown in figure 5b. This is a gray-map representation of the total retrieved phase distribution at the plane of the first test image, from which the parabolic phase of the lens has been subtracted. It can then be directly compared to the RPP pattern in figure 3a.

The supplemental information supplied by Figure 5a allows us to retrieve the RPP pattern and the phase step, within an accuracy that is limited only by the graphic representation. The phase discontinuities are also retrieved, with a spatial resolution corresponding to the sampling step of the intensity.

In order to test the algorithm with a more difficult problem, we imprinted the phase of the same RPP as in figure 3 on a beam suffering from an intrinsic strong aberration. This is simulated by a smooth transverse phase distribution whose selfcorrelation diameter and standard deviation are equal to $s_{\text{corr}} = 1$ cm and $\sigma_\phi = \pi$ respectively. Such parameters have been chosen in order to match the RPP cell size $s_{\text{cell}} = 1$ cm and phase step $\Delta\phi = \pi$. As a consequence, the spreading effect of the phase aberration on the beam propagation is comparable with that of the phase plate. As shown in figure 6a, the total phase of the input beam is the sum of this smooth aberration with the discrete RPP pattern. The code has in this order to retrieve a phase distribution with values in the interval $[0, 2\pi]$ and step discontinuities.

Three images are taken at the same positions as above, and for the same focal length and beam diameter. From these images a phase is retrieved as shown in Figure 6b. By comparing Fig. 6a with Fig. 6b, one can immediately verify that the total phase distribution has been retrieved.

The phase resolution of the algorithm has been checked with the same Gaussian beam as for figures 2 and 5 and with the RPP pattern shown in figure 3a. This time the RPP phase step $\Delta\phi$ has been varied. With simulated input images, phase steps lower than $\Delta\phi = 2\pi/100$ have been successfully retrieved. On the other hand, our simulated images were defined with an unreal-

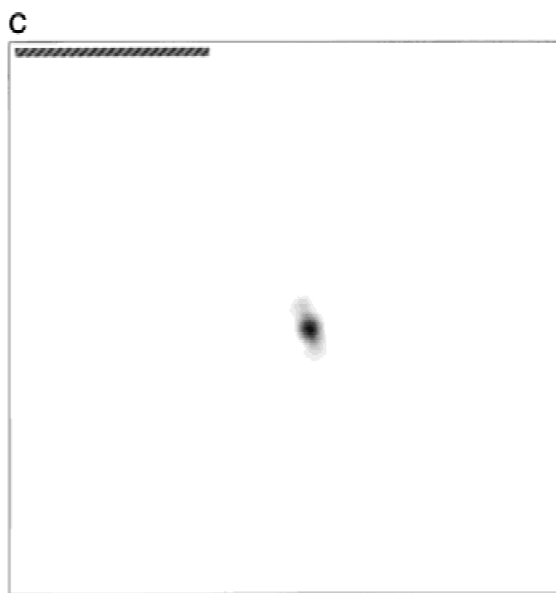


FIGURE 7. (Continued.)

istically large dynamic range. Images coming from CCD cameras are typically recorded within a dynamic range of 256 levels, for conventional linear CCDs (8-bit), or 16,384 levels, for typical cooled CCDs (14-bit). When a small $\Delta\phi$ is imposed, the total wave can be thought as the superposition of two beams. The first beam represents the 0th order of diffraction, carries the most power, and is focused within the diffraction limit. The second beam contains the higher orders of diffraction, has low power and is spread out by diffraction. As a consequence, when the level ratio of the two beams falls out of the dynamic range of the imaging system, the effect

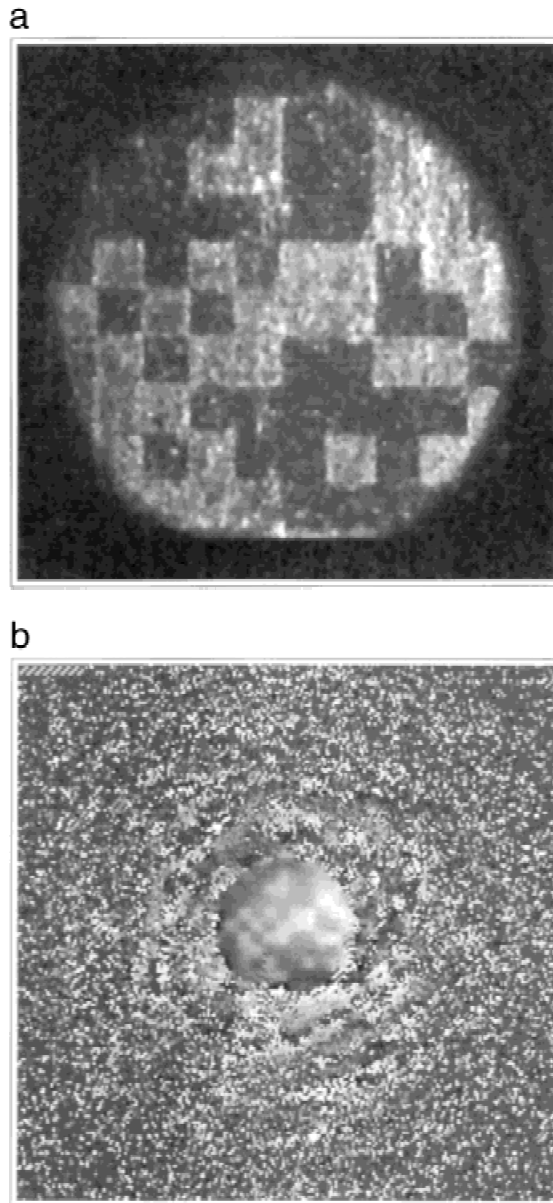


FIGURE 8. (a)—RPP scattered light image; (b)—retrieved phase at the plane of the RPP. (a)—cell size $s = 0.1$ cm; phase step $\Delta\phi = 2.0$. (b)—reference bar length $l_{\text{bar}} = 5$ cm; gray-map $[-\pi, \pi] \rightarrow [\text{white}, \text{black}]$. The retrieved phase in (b) does not contain the parabolic phase of the lens. A phase step $\Delta\phi_{\text{retr}} = 1.9 \pm 0.27$ is retrieved from (b).

of the phase perturbation is intrinsically neglected. With the given beam and phase plate, the simulations revealed a phase resolution $\delta\phi = 2\pi/5$ for 8-bit CCD cameras and $\delta\phi = 2\pi/40$ for 14-bit ones.

5. Experimental test of phase retrieving

An experimental test of this technique has been performed. The experimental scheme is the same as for the previous simulated tests. A He-Ne laser beam ($\lambda = 633$ nm) is spatially filtered before the focusing lens in order to remove intrinsic phase aberrations. Then a circular iris tailors a steep edged, flat top portion of the intensity distribution with diameter $d_{\text{in}} = 2$ cm. The beam is focused with a $f = 80$ -cm lens and passes through a RPP, whose cell size and phase step are $s_{\text{cell}} = 0.1$ cm and $\Delta\phi = 2.0$ respectively. With an 8-bit CCD digitized camera, we took the three images of the beam that are shown in figure 7. With respect to the RPP plane, the positions of the imaged planes are $z_1 = 0$, $z_2 = 77.5$ cm and $z_3 = 79.95$ cm. A scattered light image of the RPP is shown in Figure 8a, and can be compared to the retrieved phase in figure 8b. The RPP pattern is retrieved by the code with smooth edges and with a phase step $\Delta\phi_r = 1.9 \pm 0.27$.

Several reasons can explain the less accurate agreement between the input and the retrieved phase for this experimental test, when compared to the simulated test. Among the intrinsic problems of the technique, one must cite the electronic noise of the CCD camera and the lack of an absolute alignment of the three images. In this case, the noise affects the lowest ten levels of the CCD output and is partially reduced by averaging over three samples. The alignment of the centers of mass of the intensity distributions of the three images has been performed numerically and thus suffers from the residual electronic noise. Finally, a very accurate calibration of the CCD response has been necessary. Since more experimental problems affect this example, like beam doubling by double reflection in the protective glass of the CCD, we can state that simple improvements will give even better results in further experiments.

Nonetheless, due to the redundant information carried by three images, the code could discard the noise and effectively retrieve the complex field of the beam. Improved results can be obtained by comparing four images or more.

6. Conclusion

We tested a code employing the Gerchberg–Saxton algorithm as a phase retrieving technique from images. In a test situation, where a phase plate is put on a laser beam in the near-field region, we could retrieve the phase distribution of the plate with excellent agreement. With a typical imaging system dynamic range (14 bits), runs of the code on simulated images showed high phase resolution ($\pi/40$). The experimental implementation of the technique has begun with very good results. Practical problems have been pointed out in image alignment, noise reduction, and CCD camera calibration. With a much reduced experimental work, this technique can give as accurate results as interferometry. We plan to apply numerical phase retrieving to the study of short laser pulse propagation in plasmas.

Acknowledgments

We want to thank J.P. Geindre for the enlightening and encouraging discussions. One of the authors (P.C.) wants to thank the EC network “Generation and application of extra-short X-Ray pulses” for supporting his work.

REFERENCES

- BORGHESI, M. *et al.* 1997 *Phys. Rev. Lett.* **78**, 871.
- FIENUP, J.R. 1982 *Appl. Opt.* **21**, 2758.
- FIENUP, J.R. & WACKERMAN C.C. 1986, *J. Opt. Soc. Am. A* **3**, 1897.

- GERCHBERG, R.W. & SAXTON, W.O. 1972 *Optik* **35**, 237.
- GIULIETTI, D. et al. 1994 *Opt. Comm.* **106**, 52.
- GIZZI, L.A. et al. 1994 *Phys. Rev. E* **49**, 5628.
- IVANOV, V.YU. et al. 1992 *J. Opt. Soc. Am. A* **9**, 1515.
- LE BLANC, S.P. et al. 1993 *J. Opt. Soc. Am. B* **10**, 1801.
- KATO, Y. et al. 1984 *Phys. Rev. Lett.* **53**, 1057.
- MALEKI, M.H. & DEVANEY, A.J. 1993 *J. Opt. Soc. Am. A* **10**, 1086.
- MARQUÈS, J.R. et al. 1997 *Phys. Rev. Lett.* **78**, 3463.
- PEPLER, D.A. et al. 1993 *Proc. SPIE* **1870**, 76.
- TREBINO, R. & KANE, D.J. 1993 *J. Opt. Soc. Am. A* **10**, 1101.